Proceedings of ASME Turbo Expo 2011
GT2011
June 6-10, 2011, Vancouver, British Columbia, Canada

GT2011-46835

PASSIVE CONTROL OF NOISE AND INSTABILITY IN A SWIRL-STABILIZED COMBUSTOR WITH THE USE OF HIGH-STRENGTH POROUS INSERT

Daniel Sequera and Ajay K. Agrawal
Department of Mechanical Engineering
University of Alabama, Tuscaloosa, AL 35406

ABSTRACT

Swirl-stabilized combustion and porous inert medium (PIM) combustion are two methods that have been used extensively, although independently, for flame stabilization. In this study, the two concepts are combined so that the porous insert serves as a passive device to mitigate combustion noise and instabilities. A properly shaped PIM is placed within the combustor to directly influence the turbulent flow field and vortical and/or shear layer structures associated with the outer recirculation zone and inner recirculation zone. After presenting the concept, the paper provides a conceptual understanding of the changes in the mean flow field caused by the PIM. Combustion experiments were conducted at atmospheric pressure using HfC/SiC coated open-cell foam structures of different pore sizes and shapes. Measurements of sound pressure level (SPL) and CO and NOx emissions were taken for different equivalence ratios and reactant flow rates. Combustion mode and PIM geometry to decrease the SPL are identified. Results show that the porous insert can reduce combustion noise without adversely affecting NOx and CO emissions. Experiments show that the proposed concept can also mitigate combustion instabilities encountered at high reactant flow rate.

NOMENCLATURE

A	= model constant
C_D	= turbulent length scale constant
$\tilde{c}$	= progress variable
ID	= inside diameter
l_t	= turbulent length scale
OD	= outside diameter
PIM	= porous inert medium
ppcm	= pores per cm
Q	= air flow rate
S_c	= reaction progress variable source term
Sc_t	= turbulent Schmidt number
slpm	= standard liters per minute
T_i	= air inlet temperature
U_l	= laminar flame speed
U_t	= turbulent flame speed
u'	= RMS velocity
v	= velocity
Y_i	= mass fraction of product species *i*
$Y_{i,\,eq}$	= equilibrium mass fraction of product species *i*
α	= thermal diffusivity of unburnt mixture
ε	= turbulence dissipation rate
k	= turbulent kinetic energy
μ_t	= turbulent viscosity
Φ	= equivalence ratio
ρ	= density
ρ_u	= density of unburnt mixture

INTRODUCTION

In recent years, noise emission has become increasingly important to industry and society. Combustion is a common source of noise production in gas turbines, internal combustion engines, industrial burners, and commercial furnaces. Heat release in a reacting mixture causes dilatation to produce pressure pulsations, which propagate outside the flame zone as sound waves. Most practical combustion systems involve turbulent flows with embedded reaction zones that alter the noise production mechanism. In addition to the direct noise produced in the reaction zone, thermal non-uniformities in the combustor can generate indirect noise in downstream components. The topic of this study is the direct combustion noise, which is often the dominant component of the total sound power. The early research on combustion noise is summarized by Putnam [1] and Strahle [2], who report analytical models and empirical database for sound pressure level (SPL) as function of burner geometry, reactant flow rates, fuel type, equivalence ratio, etc. In recent years, research focus has shifted to Lean Premixed (LPM) combustion systems, driven by the need to comply with the increasingly stringent emissions regulations. However, typical

LPM combustion systems are prone to not only the combustion noise but also combustion instability characterized by coherent, fixed frequency feedback oscillations.

In a typical swirl-stabilized LPM combustor, reactants enter through an annular swirler, imparting swirling motion to the annular jet resulting in a compact reaction zone. The annular jet undergoes sudden expansion at the dump plane of the combustor, whereby an outer recirculation zone (ORZ) and an inner recirculation zone (IRZ) are formed on either side of the jet [3, 4]. These recirculation zones trap hot products, which ignite the fresh reactants in the annular jet to sustain the combustion process. Instantaneous flow structure within the recirculation zones is highly unsteady, with vortical structures of a wide range of length and time scales [5, 6]. Note that the vortical structures are formed in the shear layer(s) between the high-speed incoming fuel-air mixture and low-speed recirculating combustion products [7]. Formation of these flow structures is affected by the dump ratio among other geometric and operating parameters [8].

Combustion noise and instability are distinct outcomes, yet they both arise from the same source, i.e., heat release fluctuations in a turbulent flow with multiple length and time scales. According to Rayleigh's criterion [9], combustion instability occurs if the heat release process adds energy to the acoustic field faster than it can dissipate it via, for example, viscous dissipation and heat transfer. Inherently unsteady vortical structures tend to drive pressure oscillations, affecting combustion instability [10]. The approach presented in this paper seeks to suppress combustion instabilities by affecting the turbulent flow and heat release processes.

In recent years, several experimental and computational studies have sought to understand combustion noise generation mechanisms [11-20]. In particular, the advent of computational fluid dynamics (CFD) has afforded the opportunity to analyze noise generation mechanism by incorporating detailed physics of turbulent combustion and acoustics. These studies have identified passive and active methods to control combustion noise and instabilities. The effectiveness of an active combustion control system depends upon actuation, sensing, and control algorithms, among other factors. In spite of the significant progress in these areas, complete reliability of active combustion control systems is still a major concern since an unexpected event can destroy the combustor within a fraction of a second. In this study, we are exploring a passive technique to suppress the combustion noise and/or instability.

Passive techniques include baffles aimed at suppressing the acoustic standing wave, damping and dissipation through acoustic liners and Helmholtz resonators, and introduction of quarter-wave tube to interfere with the interactions between acoustics and combustion [20-23]. When pressure oscillations occur, the acoustic energy is dissipated as the flow enters and exits the damping element. Richards et al. [20] point out that the simplest acoustic damper is a hole, releasing acoustic energy from the combustion chamber that would otherwise return to the feedback loop. They quote the humorous anecdote of Putnam [1] "To solve an oscillating combustion problem, drill a hole. If that doesn't work, drill two holes." Richards et al. [20] point out that the LPM gas turbine combustors tend to have instability problems because of the absence of the numerous dilution holes present in earlier diffusion flame combustors.

Recently, we have developed a passive technique to suppress combustion noise in a swirl-stabilized, LPM combustor using an in-situ passive device [24]. The device is an open-cell, reticulated structure of Porous Inert Material (PIM) alloyed with hafnium carbide/silicon carbide (HfC/SiC) to protect from high temperature oxidation in combustion by creating refractory surface oxides with operating temperature of up to 1800 °C. The porous insert is characterized by its porosity (percentage of void volume) and pore density (number of pores per unit length). The pore density is specified in terms of pores per inch (ppi) or pores per cm (ppcm). Porosity and pore density affect the flow resistance or pressure drop across the porous material [25].

The annular ring shaped PIM is placed around the flame in the swirl-stabilized combustor as shown in Fig. 1. Following Richards et al. [20], the porous insert in Fig. 1 serves as an acoustic damper with a multitude of holes to dissipate the acoustic energy generated by the swirl-stabilized flame in the center region. However, the porous insert is more than a simple acoustic damper; it also affects the combustor flow field, and thus, the location and intensity of heat release zones. The present concept differs fundamentally from PIM combustion dealing with flame stabilized either on the surface or interior of the porous foam [26-30]. Instead, the PIM is placed around the gaseous flame produced in a swirl-stabilized combustor, to synergistically improve the performance. This paper begins with CFD analysis to gain conceptual understanding of the mean flow field without and with porous insert. Next, an experimental set up to acquire acoustics and pollutant emissions data for a range of geometric and operating conditions is described. Then, results and discussions are presented followed by the conclusions of the study.

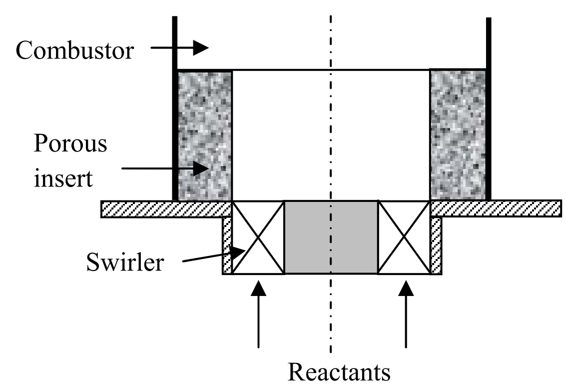

Figure 1. POROUS INSERT WITHIN A SWIRL-STABILIZED COMBUSTOR

CFD ANALYSIS

A detailed CFD analysis will demand full characterization of the wide range of length and time scales of vortical and shear layer structures in the turbulent reacting flow without and with porous insert in the combustor. However, the goal of the present analysis is to develop a preliminary insight into the mean flow field and how it is affected by the PIM. Thus, the combustor was modeled as 2D axisymetric geometry with swirl, which assumes that there are no circumferential gradients in the flow field. The flow field was computed from continuity equation and momentum equations in axial, radial and circumferential directions. Turbulence was modeled by the RNG k – ε model. Flow resistance associated with the PIM was modeled by sink terms in the momentum conservation equations. The sink term is expressed as a power law correlation with experimentally determined coefficients [25]. An effective thermal conductivity was used to account for the solid and fluid thermal conductivities weighted by the porosity of the PIM.

Combustion was modeled by turbulent premixed combustion model based on the work of Zimont et al. [31-33]. This model involves the solution of a transport equation for the reaction progress variable, with its closure based on the definition of the turbulent flame speed. The flame front propagation is modeled by solving for the density weighted mean reaction progress variable, $\tilde{c}$ [33]:

$$\nabla \cdot (\rho \vec{v} \tilde{c}) = \nabla \cdot \left(\frac{\mu_t}{Sc_t} \nabla \tilde{c} \right) + \rho S_c \quad (1)$$

where Sc_t is the turbulent Schmidt number, specified as 0.7, and S_c is the mean reaction rate (s^{-1}). The progress variable is defined as a normalized sum of the product species mass fractions [33]:

$$\tilde{c} = \frac{\sum_{i=1}^{n} Y_i}{\sum_{i=1}^{n} Y_{i,eq}} \quad (2)$$

where n is the number of product species, Y_i is the mass fraction of product species i, and $Y_{i,eq}$ is the equilibrium mass fraction of product species i. The mean reaction rate, S_c, is modeled as [33]:

$$\rho S_c = \rho_u U_t |\nabla \tilde{c}| \quad (3)$$

where ρ_u is the density of the unburnt mixture, and U_t is the turbulent flame speed given as [33]:

$$U_t = A (u')^{\frac{3}{4}} U_l^{\frac{1}{2}} \alpha^{-\frac{1}{4}} l_t^{\frac{1}{4}} \quad (4)$$

here A is the model constant (0.52), u' is the root-mean-square (RMS) velocity (m/s), U_l is the laminar flame speed (m/s), α is the thermal diffusivity of the unburnt mixture (m^2/s), and l_t is the turbulent length scale (m). Laminar flame speed and thermal diffusivity of unburnt mixture are known constants. The turbulence length scale, l_t, is computed from Eq. (5) [33]:

$$l_t = C_D \frac{(u')^3}{\varepsilon} \quad (5)$$

where ε is the turbulence dissipation rate and C_D is the turbulent length scale constant (0.37). Model constants are recommended by Zimmont et al. [33] for a wide range of turbulent premixed flames.

The computational domain extended 300 mm in the axial direction and 40 mm in the radial direction to represent the combustor. The porous insert is modeled by 40 mm ID, 80 mm OD, and 25 mm long region adjacent to the dump plane. The swirling flow at 28° angle enters the combustor at radial locations between 10 and 20 mm. Radial, axial and swirl velocity components at the inlet boundary were specified using simplified assumptions based on experimental data [34]. Axial velocity was specified as 5 m/s to correspond to the bulk inlet velocity in the experiment [5]. At the inlet, turbulence intensity was specified as 10% of the total kinetic energy and turbulent length scale was specified as 1.5 mm. The mean reaction progress variable at the inlet was specified as zero to represent the unburnt reactant mixture. Further details of the computational model are presented in Ref. 35, which also includes the grid size convergence analysis and validation tests using experimental data of Wicksall et al. [5].

The computed flow field without and with the porous insert is shown in Fig. 2 for combustion of premixed methane-air mixture at equivalence ratio, Φ = 0.58. Figure 2(a) shows that large central and corner recirculation zones are present in the mean flow field without the porous insert. In this case, the corner recirculation zone results from sudden increase of the cross-sectional area at the dump plane. The central recirculation zone is very wide, which leads to the flow tilting towards the combustor wall. With PIM, the flow structure within the combustor changes dramatically as seen in Fig. 2(b). The PIM eliminates the corner recirculation zone and creates a more uniform flow distribution. The annular jet is oriented nearly vertically, instead of inclining towards the wall for the case without the porous insert. The PIM also inhibits the radial flow and thus, much of the reacting jet flow remains within the center region.

Radial velocity profiles at different axial locations in Fig. 3 provide a direct comparison of computed flow field without and with porous insert. Without PIM, the axial velocity is negative in the corner recirculation zone, and the peak value in the flow direction shifts towards the wall. With PIM, the axial velocity peak remains at nearly a constant radial location. The axial velocity within the porous insert is nearly zero. A central region of negative axial velocities with magnitudes greater than those without the PIM indicates that the PIM intensifies the central flow recirculation region by restricting its radial spread. Figure 3(b) shows that without PIM, the swirl velocity is nearly constant in the combustor outer region, and it tends to decrease in the center region. With PIM, the swirl velocity exhibits a higher peak, which remains nearly constant in magnitude and radial location as the fluid flows in the axial direction. The swirl velocity in the porous insert is zero. Evidently, PIM helps intensify the swirl flow in the center region of the combustor. With PIM, the radial velocity decreases in the axial direction as shown in Fig. 3(c) and it is nearly zero at all axial locations. Numerical simulations of the reacting flow at an equivalence ratio of 0.85 revealed similar results. Although several assumptions were made in the present numerical study, the key results can still be interpreted qualitatively. In summary, the porous insert eliminates the corner recirculation zone, intensifies the central recirculation zone, maintains the swirling flow introduced by the swirl

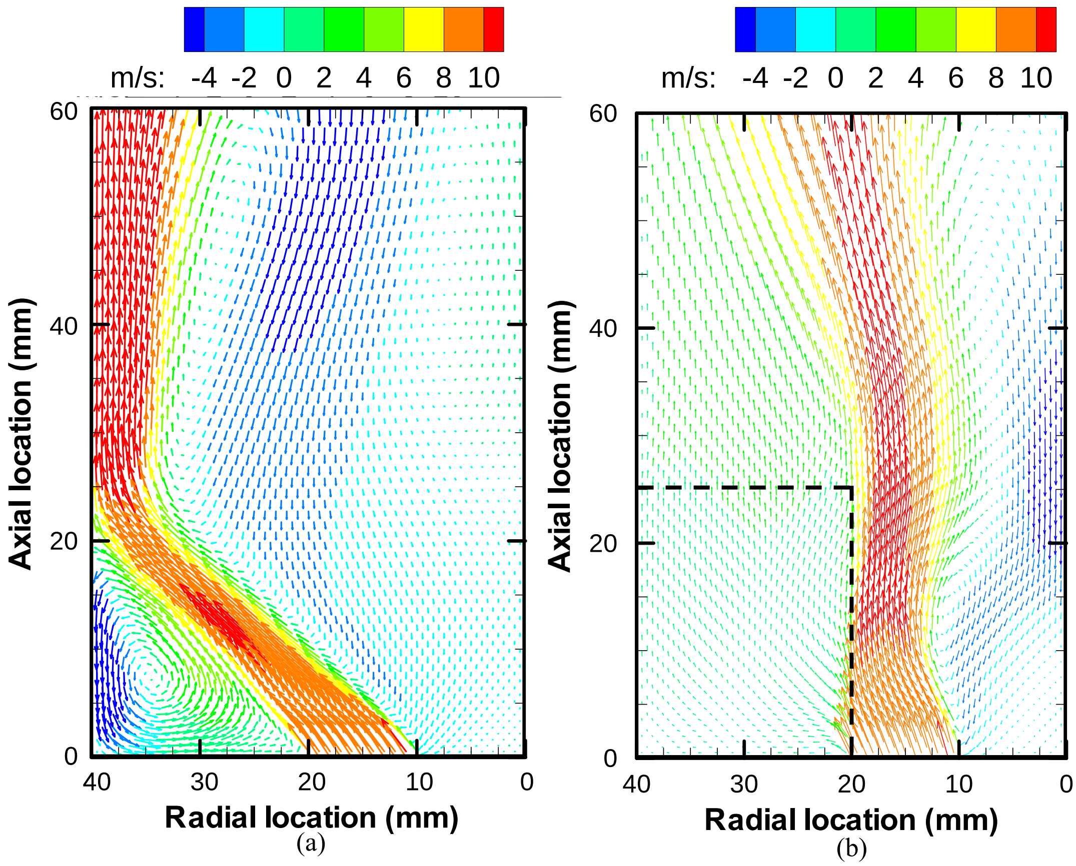

Figure 2. VELOCITY VECTORS FOR Φ = 0.58, (a) WITHOUT PIM, (b) WITH PIM

injector, and creates a more uniform flow distribution at downstream locations. These unique features of the porous insert concept greatly improve the noise and instability performance of the combustor as discussed next.

EXPERIMENTAL SETUP

Figure 4 shows the schematic diagram of the experimental setup operated at atmospheric pressure. The combustion chamber is 30.0 cm long, 8.0 cm ID quartz cylinder to enclose the flame. Heated air enters the system through a plenum filled with marbles to breakdown the large vortical structures. Combustion air passes through a swirler into the mixing section, where the gaseous methane is introduced. Air and fuel premix in the mixing region before entering the dump plane of the combustor through another swirler with six vanes positioned at 28° to the horizontal, resulting in theoretical swirl number of 1.5. The inlet Reynolds number based on the equivalent diameter of the mixing chamber ranged from 5,000 to 10,000. The combustor is back-side cooled by natural convection. A compressed storage tank supplies combustion air that passes through a pressure regulator, water traps, flow control valve, and an in-line electrical heater upstream of the experimental setup. Air flow rate is measured by a laminar flow elements (LFE) calibrated for 0 to 1000 liters per minute (lpm) of air. Methane fuel is supplied from a rack of compressed gas tanks. The LFE for the fuel flow rate measurements is calibrated for 0 to 100 lpm of methane. The flow rate measured by the LFE is corrected for temperature and pressure as specified by the manufacturer.

Sound pressure data are collected by Brüel & Kjær microphone probe (Model 4189) located 28 cm away from the edge of the combustor exit plane. A total number of 10,000 measurements are acquired in 5 sec at a sampling rate of 2,000 Hz. The measured voltage signal is converted to pressure fluctuation data using probe sensitivity of 44.3 mV/Pa. A fast-Fourier transform (FFT) analysis is performed to obtain the sound power spectra. Measurements are also processed to obtain the total sound power in decibels (dB). Emissions data are acquired by continuously sampling the product gas by a quartz probe (OD = 7.0 mm) attached to a three-way manual traversing system. The upstream tip of the probe was tapered to 1 mm ID to quench reactions inside the probe. The sample passed through an ice bath and water traps to remove moisture upstream of the gas analyzers. The dry sample reaches the electrochemical analyzers used to measure the CO and NOx concentrations in ppm. The gas analyzer also measures oxygen and carbon dioxide concentrations, used to cross-check the equivalence ratio obtained from the measured fuel and air flow rates. The uncorrected emissions data on dry basis are reported with measurement uncertainty of +/- 2 ppm.

RESULTS AND DISCUSSION

Figure 5 shows photograph of a typical porous insert characterized by thickness, ID, OD, and pore density. All

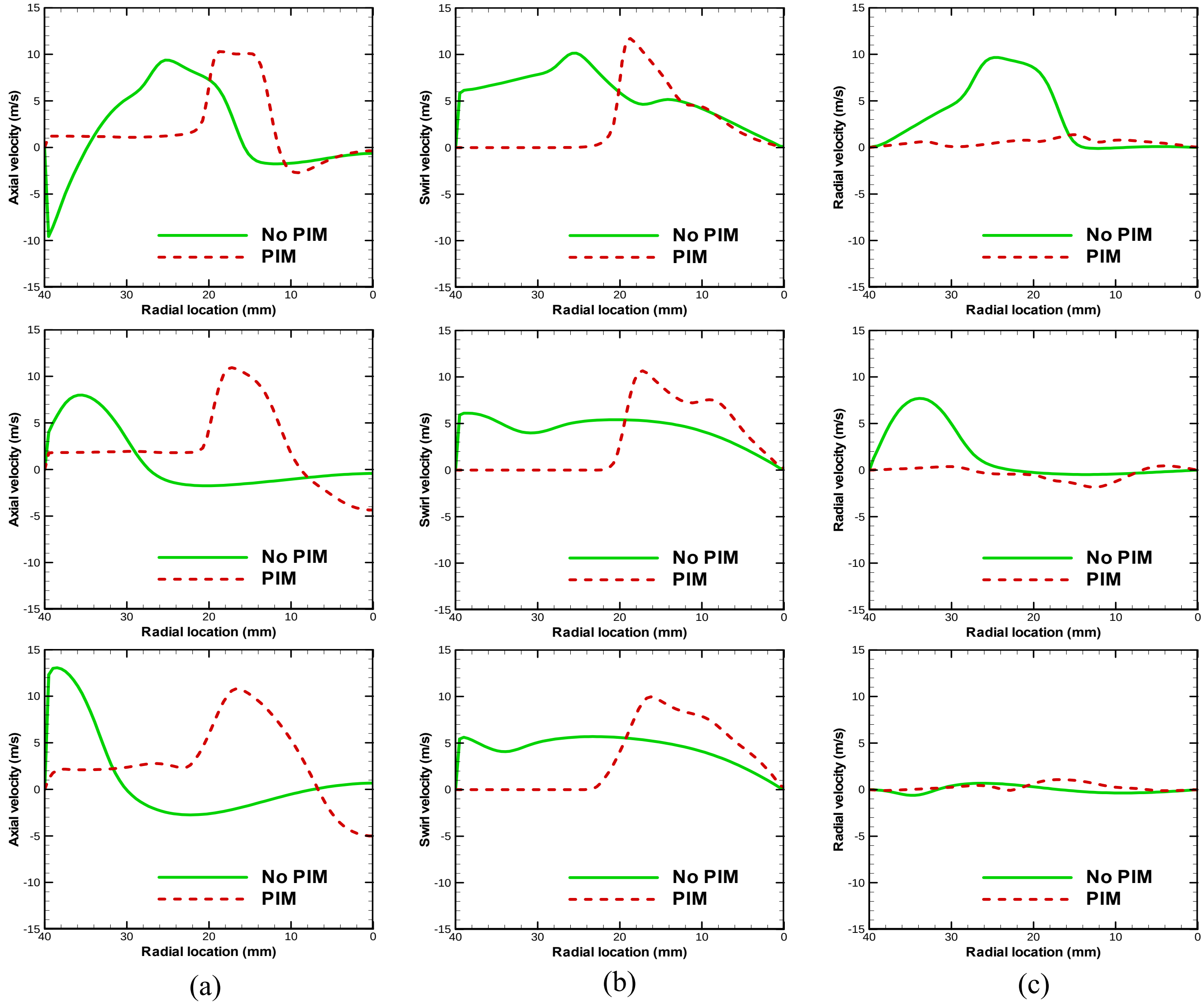

Figure 3. VELOCITY VECTORS OF REACTING FLOW AT Φ = 0.58, (a) AXIAL VELOCITY, (b) SWIRL VELOCITY, (c) RADIAL VELOCITY; AT DIFFERENT AXIAL LOCATIONS (Z): 10 mm (TOP), 20 mm (MIDDLE), 30 mm (BOTTOM)

porous inserts were 2.5 cm thick, 8.0 cm OD, and had porosity of 85%. For each experiment, two porous inserts were stacked together to create different geometric configurations. Figure 6 lists seven PIM configurations investigated in this study. The first three cases utilized porous inserts of 4, 8, and 18 ppcm. The remaining cases used 18 ppcm porous inserts with constant, increasing, or decreasing cross-sectional area in the flow direction. Experiments were conducted at Φ = 0.7 and 0.8, airflow rate, Q = 300 slpm and 600 slpm, and air inlet temperature, T_i = 100˚C and 120˚C.

Effect of PIM Pore Density

Figure 7 presents the acoustic power spectra at Φ = 0.7 for configurations A to D, i.e., without PIM and with PIM of different pore densities. Without PIM, the power spectra in Fig. 7(a) show a peak at 250 Hz and minor peaks centered around 500 Hz and 590 Hz. The PIM of 4 ppcm results in broadband power spectra with a minor peak at 250 Hz (see Fig. 7b). The PIM of 8 and 18 ppcm do not show distinct peak at any frequency. Thus, PIM is shown to suppress combustion noise and possibly mitigate combustion instability. Figure 8 shows acoustic power spectra for configurations A to D at Φ = 0.8. In this case, power spectra without PIM is broadband with much of the power centered around 500 Hz. However, a distinct peak indicating instability is observed at 450 Hz for PIM of 4 ppcm (Fig. 8b) and at 700 Hz for PIM of 8 ppcm (Fig. 8c). PIM with 18 ppcm results in a smaller peak at 250 Hz. The shift in the measured frequency with the PIM pore density might in part be affected by aliasing introduced by the low sampling rate of 2000 Hz. Although the key results are not affected, a higher sampling rate is desirable for future studies. The above results show that the porous insert could also instigate instability in an otherwise stable combustor. Flame stabilization mode with PIM is important to this anomaly as discussed next.

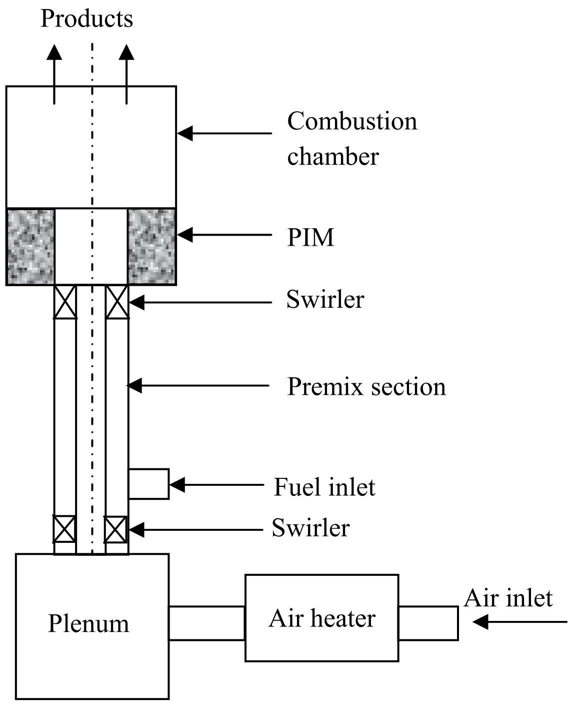

Figure 4. SCHEMATIC DIAGRAM OF EXPERIMENTAL SETUP

Figure 5. PHOTOGRAPH OF A POROUS INSERT

Configuration A Pore density: None IDs: None	None (Baseline)
Configuration B Pore density: 4 ppcm IDs: 3.8, 4.4 cm	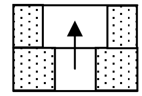
Configuration C Pore density: 8 ppcm IDs: 3.8, 4.4 cm	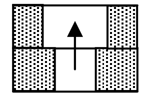
Configuration D Pore density: 18 ppcm IDs: 3.8, 4.4 cm	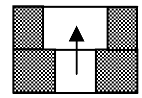
Configuration E Pore density: 18 ppcm IDs: 3.8, 5.0 cm	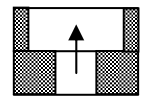
Configuration F Pore density: 18 ppcm IDs: 3.8, 3.8 cm	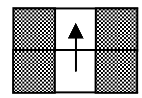
Configuration G Pore density: 18 ppcm IDs: 5.0, 5.0 cm	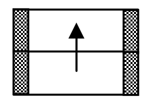
Configuration H Pore density: 18 ppcm IDs: 4.4, 3.8 cm	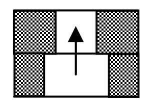

Figure 6. DESCRIPTION AND SCHEMATIC DIAGRAM OF PIM CONFIGURATIONS

Figure 9 shows visual flame images for $\Phi = 0.7$, $Q = 300$ slpm, and $T_i = 100^{\circ}C$. Image for configuration B in Fig. 9(a) shows orange glow indicative of interior combustion, i.e., combustion stabilized within the porous matrix. A confined blue gaseous swirl-stabilized flame is also visible downstream of the PIM. The image in Fig. 9(b) reveals a fundamentally different combustion mode for configuration D; small blue flamelets are stabilized on the surface of the PIM while the remaining reactants burn within the confined, swirl-stabilized gaseous flame region. Increase in acoustic power in Figs. 8(b) and 8(c) resulted from interior combustion mode, which is found to be undesirable.Table 1 presents a summary of the total SPL (in dB) for the baseline case (no PIM) and each configuration with PIM. Each datum represents the average of five independent measurements. Results show that porous insert of 18 ppcm is most effective in achieving PIM surface combustion mode, which is necessary to mitigate the combustion noise and/or instability. Porous insert of 4 ppcm resulted in interior combustion mode for both Φ. Compared to the baseline case, the total SPL decreased by 2.9 dB for $\Phi = 0.7$ but increased by 3.2 dB for $\Phi = 0.8$. Porous insert of 8 ppcm also resulted in interior combustion mode for both Φ. The total SPL decreased by 6.8 dB for $\Phi = 0.7$, but it increased by 1.0 dB for $\Phi = 0.8$. Porous insert of 18 ppcm resulted in surface combustion mode and reduction in total SPL by 7.1 dB for $\Phi = 0.7$. The total SPL for $\Phi = 0.8$ also decreased by 4.0 dB, since only a narrow downstream layer of PIM was exposed to interior combustion.

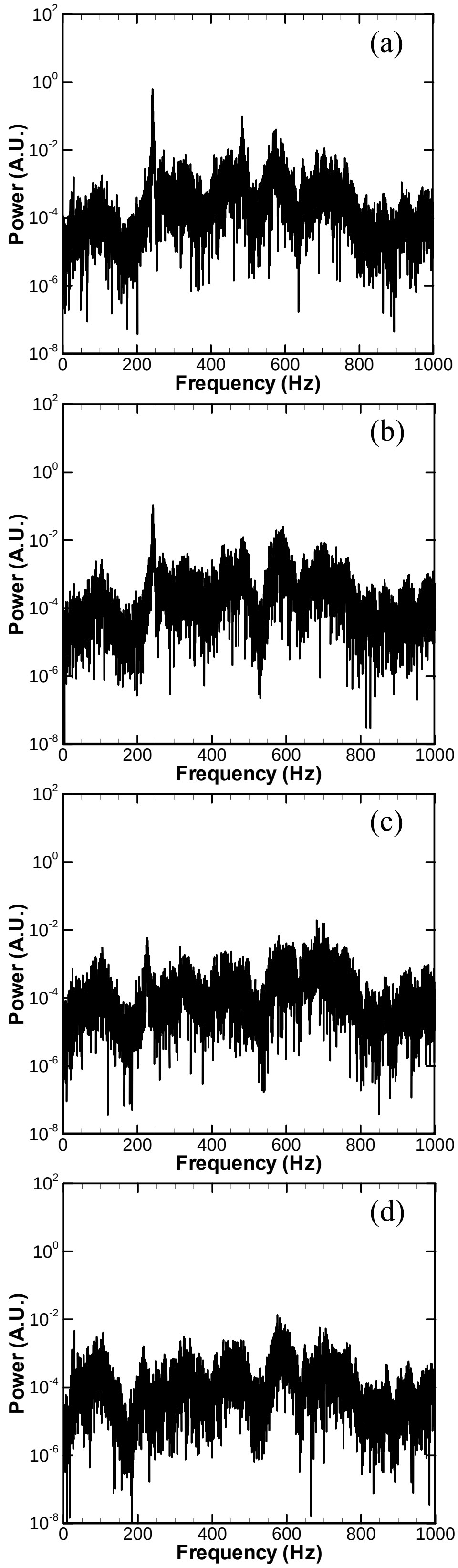

Figure 7. POWER SPECTRA FOR Q = 300 SLPM, Φ = 0.7 (a) CONFIGURATION A (b) CONFIGURATION B (c) CONFIGURATION C (d) CONFIGURATION D

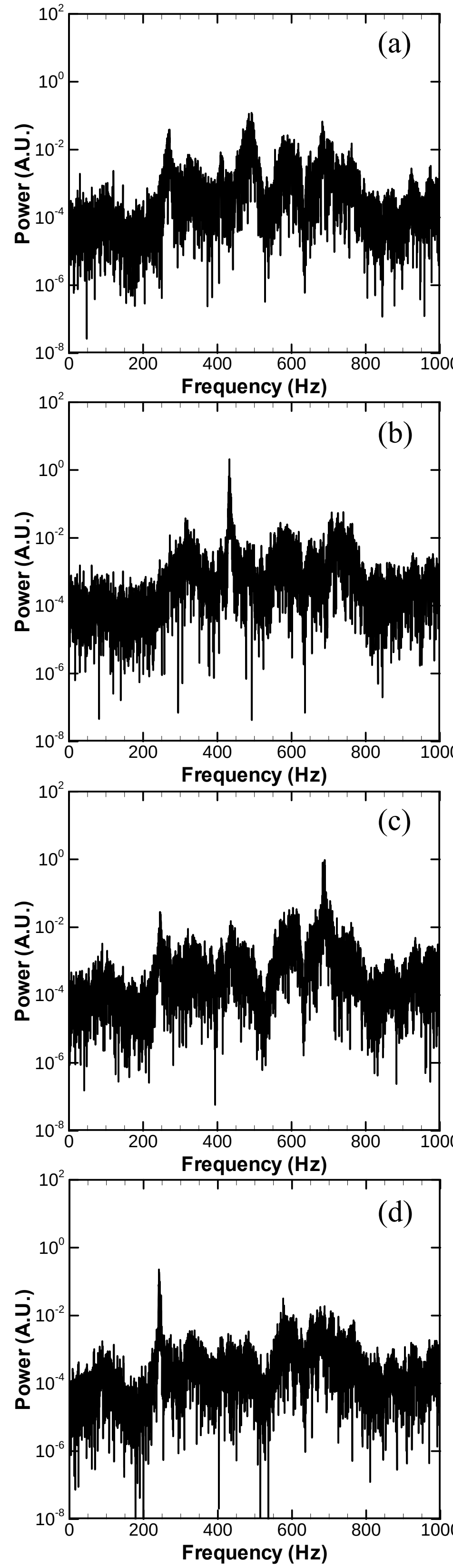

Figure 8. POWER SPECTRA FOR Q = 300 SLPM, Φ = 0.8 (a) CONFIGURATION A (b) CONFIGURATION B (c) CONFIGURATION C (d) CONFIGURATION D

Table 1. TOTAL SOUND PRESSURE FOR Q = 300 SLPM

Configuration	Φ = 0.7	Φ = 0.8
A	103.0 dB	103.9 dB
B	100.1 dB	107.1 dB
C	96.2 dB	104.9 dB
D	95.4 dB	99.8 dB
E	95.4 dB	99.9 dB
F	95.7 dB	99.8 dB
G	96.1 dB	104.8 dB
H	96.2 dB	106.8 dB

Figure 10 illustrates that the reactant flow exiting the swirl injector is divided into the center (core) region and PIM region; the reactant flow rate in the PIM region depends upon the flow resistance of the PIM. Combustion products from the free flame also enter the porous insert through the inner surface and mix with the reactants introduced upstream. Moreover, combustion products transfer heat to reactants flowing through the PIM, which would lead to interior or surface combustion depending upon the flame speed and porous insert geometry. Interior combustion occurs when reactants ignite and sustain flame within the PIM. In this case, a balance is achieved among: (1) energy of unburned reactants

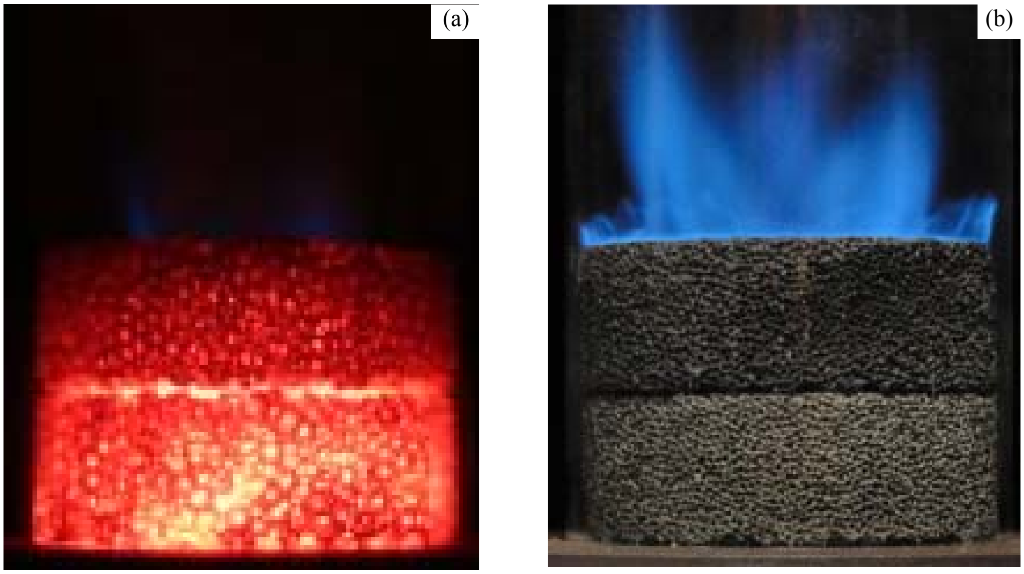

Figure 9. FLAME IMAGES (a) WITH PIM INTERIOR COMBUSTION (b) WITH PIM SURFACE COMBUSTION

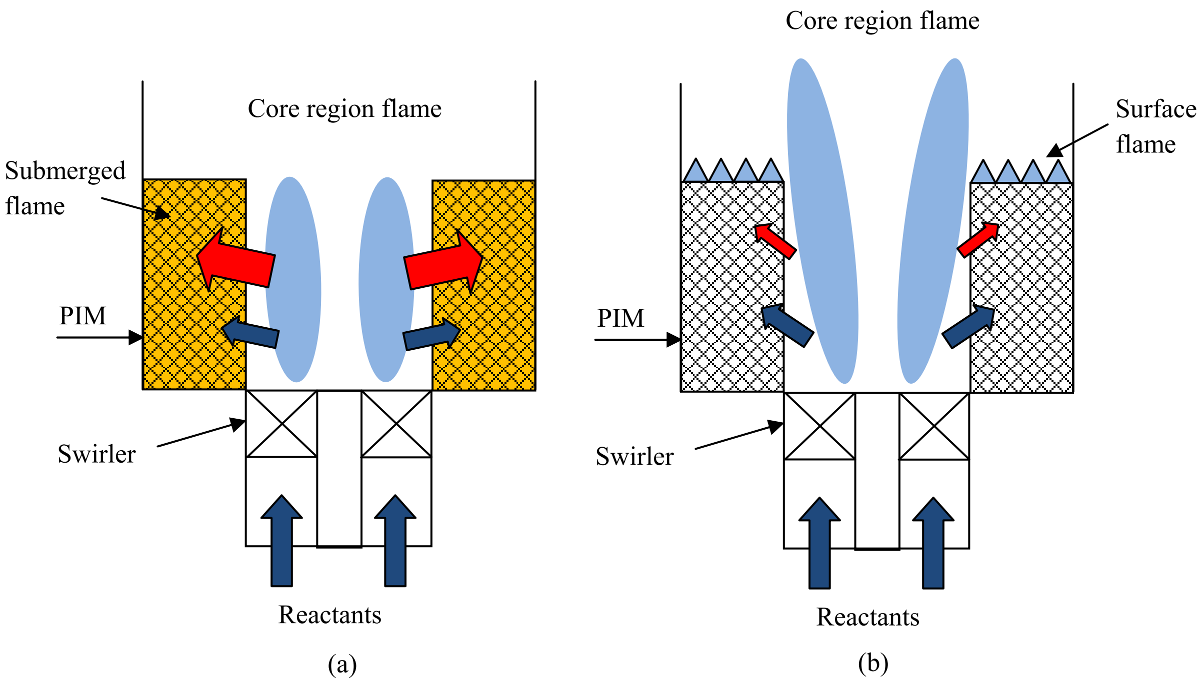

Figure 10. SCHEMATIC DIAGRAM ILLUSTRATING STABILIZATION MECHANISM (a) INTERIOR COMBUSTION (b) SURFACE COMBUSTION

flowing in the PIM, (2) energy of products from the free flame entering the PIM, and (3) heat transfer between the free flame and PIM. Porous insert with large pores favor this balance to result in interior combustion (Fig. 9a). Porous insert with small pores favors flame stabilized on the downstream surface of the PIM (Fig. 9b).

Interior and surface combustion modes excite the acoustic field differently, thus resulting in different acoustic power levels. First, the PIM serves as an acoustic damper to suppress the pressure fluctuations in the adjacent free flame. In surface combustion mode, the turbulent fluctuations in the swirl-stabilized flame are damped by the PIM since the reaction zone is located outside the PIM. In interior combustion mode, the reaction zone is located within the PIM, and thus, no effective mechanism exists to dampen the turbulent fluctuations of the swirl-stabilized flame. Second, flamelets on the downstream PIM surface distribute combustion to reduce the heat release rate in the swirl-stabilized flame. Distributed reaction zones make the coupling between pressure fluctuations and reaction zones difficult, and thus, the Rayleigh criterion is not satisfied. The interior combustion is mode is less effective since it creates intense reaction zones within the PIM. Finally, the vortical structures produced in the corner recirculation zone are eliminated by the PIM. This last comment might explain the noise reduction achieved with interior combustion mode for some of the test conditions. However, the surface combustion mode facilitates all three mechanisms identified, and thus, it is necessary to reduce noise/instability over a wide range of test conditions. Note that a non-porous block could also eliminate the corner recirculation zone. However, such a scheme does not offer the first two benefits discussed above, i.e., attenuation of pressure fluctuations produced in the swirl-stabilized flame, and distributed heat release rate across the combustor by creating surface stabilized flamelets.

Effect of PIM Shape

By changing PIM shape with a fixed pore density, the interaction between the free flame and the PIM can be tailored to favor or inhibit interior combustion. Thus, experiments were conducted with 18 ppcm porous inserts of different IDs to increase, decrease, and maintain constant flow cross-sectional area. Acoustic power spectra for Q = 300 slpm at $\Phi = 0.7$ in Fig. 11 show that configuration G is least effective in suppressing combustion noise and/or instability. This result is attributed to the increased volume of the free flame region at the dump plane, which changes the stabilization mechanism by approaching conditions similar to the baseline case, i.e., corner recirculation zone accompanied with vortical structures in the shear layer of the flame. In this case, interior combustion was observed on the inner surface of the porous insert. Similar trends were observed at $\Phi = 0.8$ as shown in Fig. 12, whereby Configuration E (increasing free flow area) and configuration F (constant area) provided the best results.

Best performing cases had no indication of interior combustion. For these cases, the ID of the upstream porous insert is the same as the OD of the swirl injector at the dump plane. Table 1 shows that the total SPL was similar for PIM configurations D, E and F; 7.0 dB reduction at $\Phi = 0.7$, and 4.0 dB reduction at $\Phi = 0.8$ compared to the baseline case without PIM. Similar to Configuration F, Configuration G uses constant ID porous inserts. However, configuration G decreased the total SPL by 6.9 dB at $\Phi = 0.7$, but increased it by 0.9 dB at $\Phi = 0.8$ because of the sudden increase in the flow area at the dump plane. PIM configuration H decreased the total SPL by 6.8 dB at $\Phi = 0.7$, but increased it by 3.9 dB at $\Phi = 0.8$. In this case, the downstream confinement of the free flame promotes flow of combustion products into the porous insert to result in interior combustion mode with poor acoustics performance.

Effect of Reactant Flow Rate

Experiments were conducted at a higher air flow rate of Q = 600 slpm and $T_i = 120^\circ C$. Figure 13 shows acoustic power spectra at $\Phi = 0.7$ for configurations A (without PIM), D (divergent), G (constant), and H (convergent). Configuration A shows a distinct peak indicating combustion instability at 520 Hz (Fig. 13a). All configurations with PIM resulted in broadband spectra, indicating that the porous insert also mitigated combustion instability. None of the flames with porous insert experienced interior combustion. In spite of the high reactant flow rate, interior combustion still occurred for some cases at $\Phi = 0.8$. Acoustic power spectra at $\Phi = 0.8$ in Fig. 14(a) reveal combustion instability at 540 Hz without PIM. Figure 14(b) shows that the spectral peak is virtually eliminated with the use of divergent PIM (configuration D), while instability is still present for PIM with constant or convergent flow cross-sectional area. Table 2 shows that at high reactant flow rate, all porous inserts were effective in reducing combustion noise/instability at $\Phi = 0.7$, with typical reductions in total SPL of 13 to 14 dB. For $\Phi = 0.8$, only the divergent configuration was effective and it reduced the total SPL by 13 dB. Configurations G and H were either ineffective or marginally effective because of their propensity for interior combustion. These results show that the porous insert can effectively mitigate combustion noise and/or instabilities when the interior combustion is avoided by a judicious choice of PIM shape and pore density.

Table 2. TOTAL SOUND PRESSURE FOR Q = 600 SLPM

Configuration	Q = 600 slpm	
	$\Phi = 0.7$	$\Phi = 0.8$
A	118.9 dB	120.5 dB
D	**105.9 dB**	**107.1 dB**
G	104.7 dB	120.4 dB
H	105.8 dB	115.1 dB

CO and NOx Emissions

Figure 15 presents radial profiles of CO and NOx concentrations at the combustor exit plane for Q = 300 slpm, $T_i = 100^\circ C$, and $\Phi = 0.8$. The CO emissions are similar for all cases, but NOx emissions are the highest for configuration G with constant area porous insert. Interestingly, NOx emissions for best performing configuration (divergent porous insert) are comparable to the case without PIM. For all cases, emissions profiles are nearly flat in the radial direction, indicating good spatial uniformity of combustion. Overall, results show that

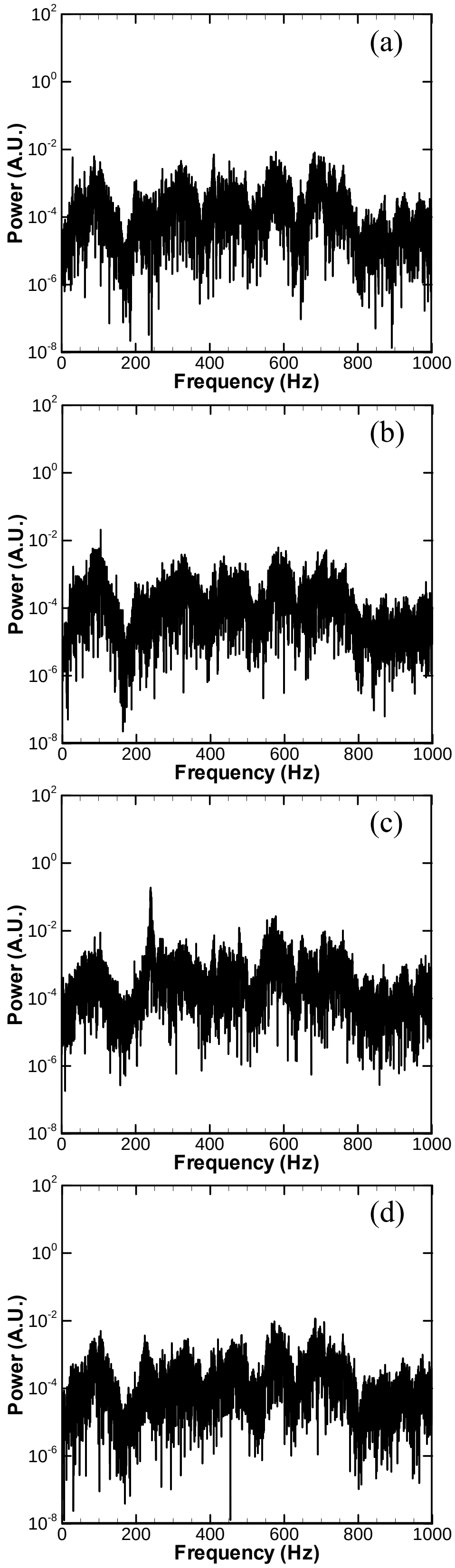

Figure 11. POWER SPECTRA FOR Q = 300 SLPM, Φ = 0.7 (a) CONFIGURATION E (b) CONFIGURATION F (c) CONFIGURATION G (d) CONFIGURATION H

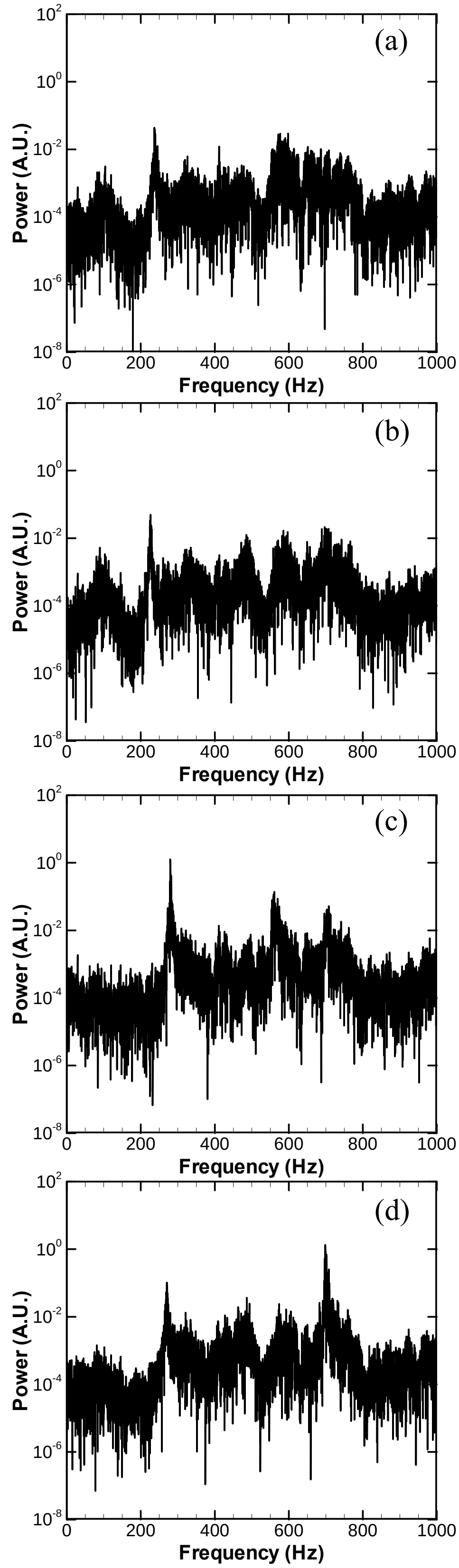

Figure 12. POWER SPECTRA FOR Q = 300 SLPM, Φ = 0.7 (a) CONFIGURATION E (b) CONFIGURATION F (c) CONFIGURATION G (d) CONFIGURATION H

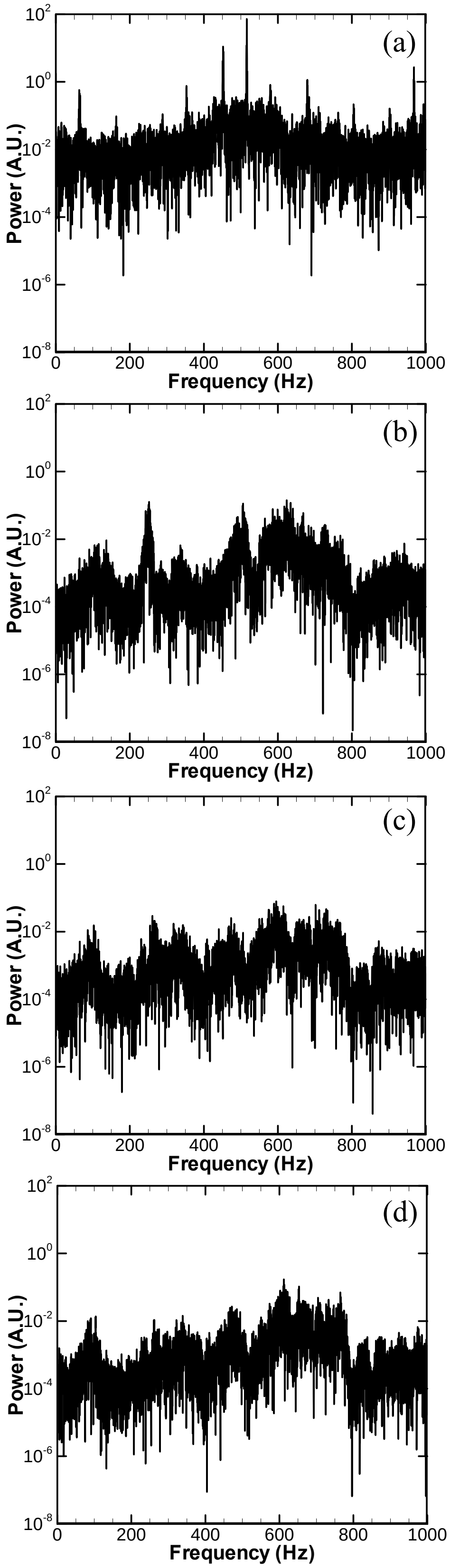

Figure 13. POWER SPECTRA FOR Q = 600 SLPM, Φ = 0.7 (a) CONFIGURATION A (b) CONFIGURATION D (c) CONFIGURATION G (d) CONFIGURATION H

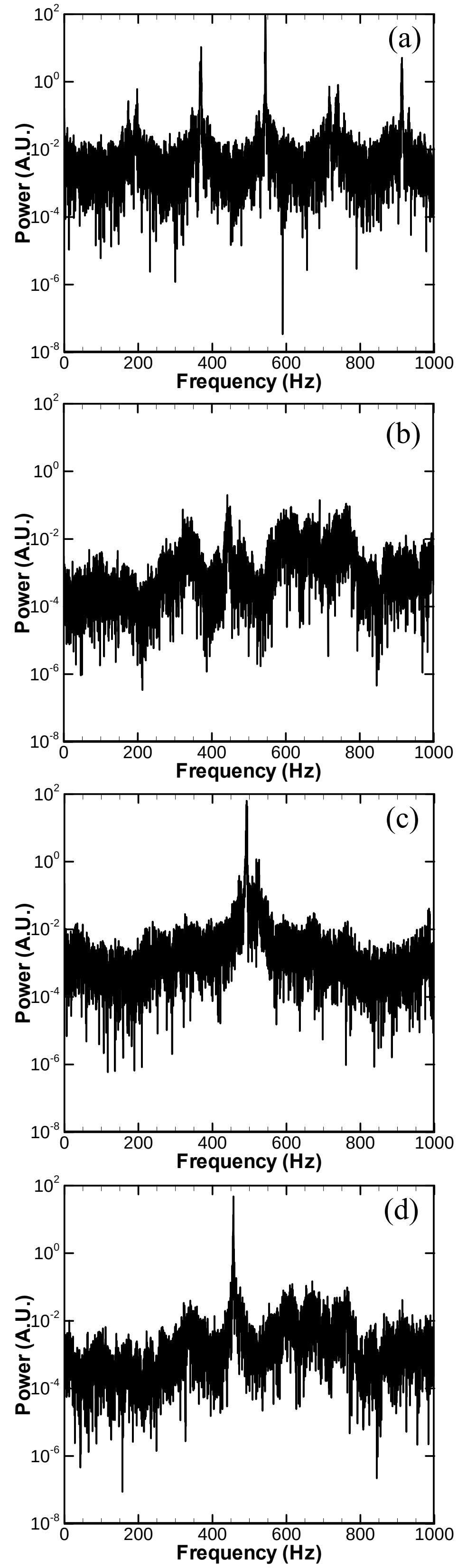

Figure 14. POWER SPECTRA FOR Q = 600 SLPM, Φ = 0.8 (a) CONFIGURATION A (b) CONFIGURATION D (c) CONFIGURATION G (d) CONFIGURATION H

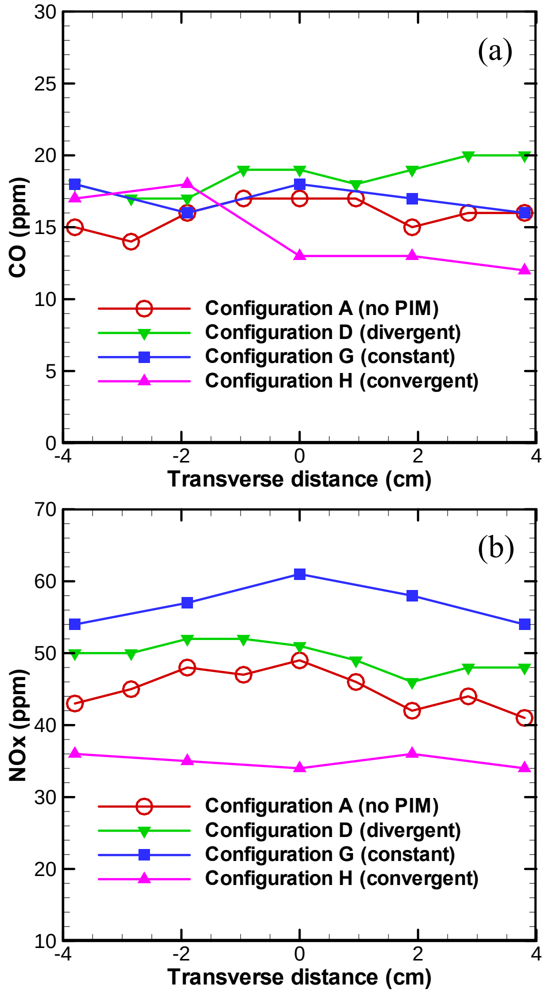

Figure 15. CO AND NOx EMISSIONS FOR Q = 300 SLPM, Φ = 0.8, T_i = 100°C (a) CO (b) NOx

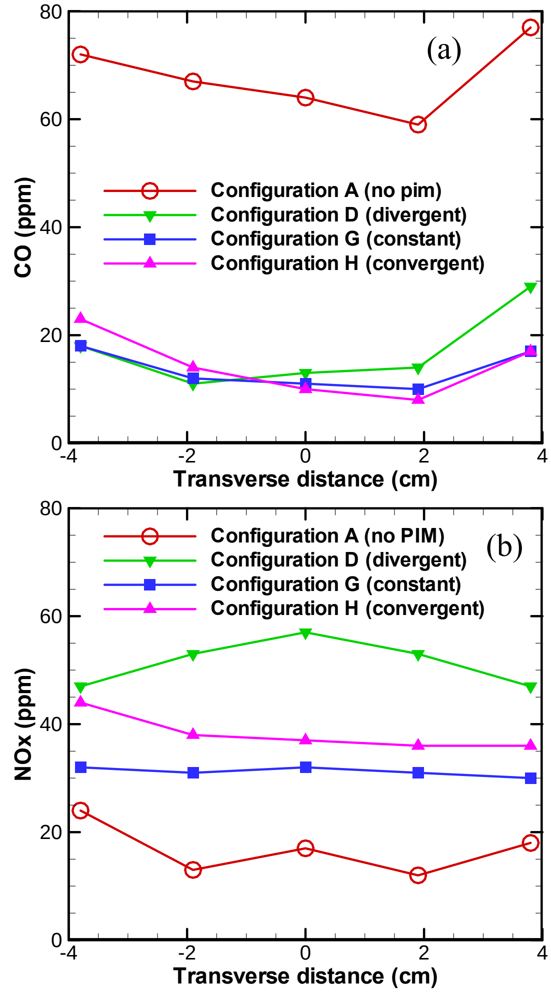

Figure 16. CO AND NOx EMISSIONS FOR Q = 600 SLPM, Φ = 0.8, T_i = 120°C (a) CO (b) NOx

the porous insert does not have an adverse effect on CO and NOx emissions. Finally, Fig. 16 shows CO and NOx emissions at the combustor exit plane for Q = 600 slpm, T_i = 120˚C, and Φ = 0.8. Fig. 16(a) shows that the CO emissions without the PIM vary from 60 to 80 ppm. With PIM, the CO emissions decrease significantly to below 30 ppm for all porous inserts. Figure 16(b) shows that the NOx emissions increase with the porous insert, an observation requiring further investigation and optimization. Overall, results are very encouraging and suggest that significant reductions in combustion noise, combustion instability, and pollutant emissions are feasible by a judicial choice of porous insert placed within the swirl-stabilized combustor.

Long Duration Experiments

The porous insert has been shown to operate reliably for several hours in the combustor. The combustor was operated continuously for 4-hour period using Configuration D (divergent) because of its optimum performance reported in the previous section. The objective was to test material endurance over several hours of operation, and to identify structural damage if any, and its effect on combustion noise, combustion instability, and CO and NOx emissions. Measurements were taken at 30 minute intervals for Q = 600 slpm and Φ = 0.7. Results showed steady combustion process throughout the test duration as documented by nearly constant total SPL and emissions data throughout the test. The porous material did not reveal any detectable change after use.

CONCLUSIONS

In this study, swirl stabilization mechanism in lean premixed combustion is manipulated by a porous insert to reduce combustion noise and/or instability without adversely affecting CO and NOx emissions. The approach involves passive control of flow structures that generate noise in the combustion chamber. The proposed technique can also mitigate combustion instabilities that self-excite within the combustor by proving an acoustic damper around the reaction zone. A numerical simulation of non-reacting and reacting flows was performed to gain qualitative understanding of the flow structure without and with porous insert. Next, an experimental investigation was conducted to determine how PIM shape and pore-density affected the sound pressure level. The numerical study shows that the porous insert eliminates the corner recirculation zone, strengthens the center recirculation zone, and creates a more uniform flow distribution at the downstream locations. These flow structure changes improve noise and instability performance of combustor. Experimental study identified interior and surface combustion modes with porous insert. Geometric parameters of the porous insert such as pore density and PIM shape affected the combustion mode. Surface combustion mode is desirable, while interior combustion must be avoided to reduce the total sound pressure levels. Porous insert of large pore density (18 ppcm) and diverging flow cross-sectional area was found to provide the best performance. Unlike typical porous ceramics, the HfC/SiC coated porous insert used in this study provides excellent structural strength in the high temperature reacting environment of gas turbine combustion systems. The present strategy can be readily implemented in can-type gas turbine combustion systems. Present/future work is focused on experiments at higher reactant flow rates, higher reactant inlet temperatures, and higher operating pressure to more closely replicate the gas turbine operating conditions. Ongoing/future tasks also include longer duration tests (>10 hours) to document sustained operation without deterioration in performance and/or porous materials properties, and integration of porous material with combustor.

ACKNOWLEGEMENTS

This research was supported by the Office of Naval Research through an SBIR award to the Ultramet Corporation. Dr. Gabriel Roy served as the technical monitor.

REFERENCES

[1] Putnam, A.A., 1971. *Combustion Driven Oscillations in Industry*, Elsevier, New York.

[2] Strahle, W.C., 1978. "Combustion Noise". *Progress in Energy and Combustion Science*, **4**(3), pp. 157–176.

[3] Schefer, R.W., Wicksall, D.M., and Agrawal, A.K., 2002. "Combustion of hydrogen-enriched methane in a lean premixed swirl-stabilized burner". *Proceedings of the Combustion Institute*, **29**(1), pp. 843-851

[4] Lieuwen, T.C., and Yang, V., ed., 2005. *Combustion Instabilities in Gas Turbine Engines*, Vol 210. Progress in AIAA.

[5] Wicksall, D.M., Agrawal, A.K., Schefer, R.W., and Keller, J.O., 2005. "Influence of Hydrogen Addition on Flow Structure in Enclosed Swirling Methane Flame". *Journal of Propulsion and Power*, **21**, pp. 16-24.

[6] Wicksall, D.W., Agrawal, A.K., Schefer, R.W., and Keller, J.O., 2005. "The Interaction of Flame and Flow Field in a Lean Premixed Swirl-Stabilized Combustor Operated on H_2/CH_4/Air". *Proceedings of the Combustion Institute*, **30**, pp. 2875-2883.

[7] Schadow, K. C. and Gutmark, E., 1992. "Combustion Instability Related To Vortex Shedding in Dump Combustors and their Passive Control". *Progress in Energy and Combustion Science*, **18**, pp. 117-132.

[8] Huang, Y., and Yang, V., 2009. "Dynamics and stability of lean-premixed swirl-stabilized combustion". *Progress in Energy and Combustion Science*, **35** (4), pp. 293-364.

[9] Rayleigh, J.S.W., 1945. *The Theory of Sound*, Vol. 2, Dover, New York.

[10] Schadow, K. C., Gutmark, E., Wilson, K. J., and Smith, R. A., 1988. "Multistep Dump Combustor Design to Reduce Combustion Instabilities". AIAA/ASME/SAE/ASEE 24th Joint Propulsion Conference, Paper 88-2854.

[11] Schwarz, A. and Janicka, J., ed., *Combustion Noise*. Springer, 2009.

[12] Rajaram, R., Gray, J., and Lieuwen, T., 2006. "Premixed Combustion Noise Scaling: Total Power and Spectra". AIAA paper 2006-2612.

[13] Flemming, F., Olbrit, C., Wegner, B., Sadiki, A., Janicka, J., Bake, F., Michael, U., Lehmann, B., and Rohle, I., 2005. "Analysis of Unsteady Motion with Respect to Noise Sources in a Gas Turbine Combustor: Isothermal Flow Case". *Flow, Turbulence and Combustion*, **75**, pp. 3-27.

[14] Choi, G., Tanahashi, M., and Miyauchi, T., 2005. "Control of Oscillating Combustion and Noise Based on Local Flame Structure". *Proceedings of the Combustion Institute*, **30**, pp. 1807-1814.

[15] Hirsch, C., Wasle, J., Winkler, A., and Sattelmayer, T., 2007. "A Spectral Model for the Sound Pressure from Turbulent Premixed Combustion". *Proceedings of the Combustion Institute*, **31**, pp. 1435-1441.

[16] Tiribuzi, S., 2008. "CFD Simulation of Noise in Gas Turbine Combustors by Means of Turbulence Refluctuation Method". *Proceedings of ASME Turbo Expo*, **3**, pp. 113-124.

[17] Duchaine, P., Zimmer, L., and Schuller, T., 2009. "Experimental Investigation of Mechanisms of Sound Production by Partially Premixed Flames". *Proceedings of the Combustion Institute*, **32**, pp. 1027-1034.

[18] Lee, J.G., and Santavicca, D.A., 2003. "Experimental Diagnostics for the Study of Combustion Instabilities in Lean Premixed Combustors". *Journal of Propulsion and Power,* **19**(5), pp. 735-750.

[19] Noiray, N., Durox, D., Schuller, T., and Candel, S., 2009. "Dynamic Phase Converter for Passive Control of Combustion Instabilities". *Proceedings of the Combustion Institute*, **32**, pp. 3163-3170.

[20] Richards, G.A., and Straub, D.L., 2003. "Passive Control of Combustion Dynamics in Stationary Gas Turbines". *Journal of Propulsion and Power*, **19**(5), pp. 795-810.

[21] Sreenivasan, K.R., and Raghu, S., 2000. "The Control of Combustion Instability: A Perspective". *Current Science*, **79**, pp. 867-883.

[22] Steele, R.C., Cowell, L.H., Cannon, S.M., and Smith C.E., 2000. "Passive Control of Combustion Instability in Lean Premixed Combustors". *Journal of Engineering for Gas Turbines and Power*, **122**, pp. 412-419.

[23] Huang, Y., and Yang, V., 2009. "Dynamics and Stability of Lean-Premixed Swirl-Stabilized Combustion". *Progress in Energy and Combustion Science*, **35**, pp. 293-364.

[24] Agrawal, A.K., and Vijaykant, S., 2010. Passive Noise Attenuation System, U.S. Patent Application Publication No. US2010/0059311A1, March.
[25] Marbach, T. and Agrawal, A.K., 2005. "Experimental Study of Surface and Interior Combustion using Composite Porous Inert Media". *Journal of Engineering for Gas Turbines and Power,* **127**, pp. 307-313.
[26] Howell, H.R., Hall, M.J., and Ellzey, J.L., 1996. "Combustion of Hydrocarbon Fuels within Porous Inert Media". *Progress in Energy and Combustion Science*, **22**, pp. 121 – 145.
[27] Trimis, D., and Durst, F., 1996. "Combustion in a Porous Medium – Advances and Applications". *Combustion Science and Technology*, **121**, pp. 153-168.
[28] Marbach, T.L., Sadasivuni, V., and Agrawal, A.K., 2007. "Investigation of a Miniature Combustor Using Porous Media Surface Stabilized Flame". *Combustion Science and Technology*, **179**(9), pp. 1901-1922.
[29] Waitz, I.A., Gauba, G., and Tzeng, Y.S., 1998. "Combustors for Micro-gas Turbine Engines". *Journal of Fluids Engineering,* **120**, pp. 109 – 117.
[30] Fernandez-Pello, A.C., 2002. "Micropower Generation Using Combustion: Issues and Approaches". *Proceedings of the Combustion Institute*, **29**, pp. 883 – 899.
[31] Zimont, V., 2000. "Gas Premixed Combustion at High Turbulence. Turbulent Flame Closure Model Combustion Model". *Experimental Thermal and Fluid Science*, **21**, pp. 179-186.
[32] Zimont, V.L., and Lipatnikov, A.N., 1995. "A Numerical Model of Premixed Turbulent Combustion of Gases". *Chemical Physics Report*, **14**(7), pp. 993-1025.
[33] Zimont, V., Polifke, W., Bettelini, M., and Weisenstein, W., 1998. "An Efficient Computational Model for Premixed Turbulent Combustion at High Reynolds Numbers Based on a Turbulent Flame Speed Closure". *Journal of Gas Turbine Power*, **120**, pp. 526-532.
[34] Gupta, A.K., Lilley, D.G., and Syred N., 1984. *Swirl Flows*. Abacus Press, Tunbridge Wells, England.
[35] Sequera, D., and Agrawal, A.K., 2009. "Numerical Simulations of Swirl-Stabilized Combustion Coupled with Porous Inert Medium". Proceedings of the 6th U.S. National Combustion meeting, Paper 11C3.